Colloids and Surfaces A: Physicochem. Eng. Aspects 506 (2016) 840–848

Contents lists available at ScienceDirect

Colloids and Surfaces A: Physicochemical and Engineering Aspects

journal homepage: www.elsevier.com/locate/colsurfa

Porous $LaFeO_3$/Silica Nanocomposites via Sol-Gel Mixing Involving Citric Acid

Kamal M.S. Khalil[a,*], Walaa A. Elhamdy[a], Abd El-Aziz A. Said[b], Ahmed A. Elsamahy[a]

[a] Chemistry Department, Faculty of Science, Sohag University, P.O. Box. 82524 Sohag, Egypt
[b] Chemistry Department, Faculty of Science, Assiut University, P.O. Box 71516 Assiut, Egypt

HIGHLIGHTS

- $LaFeO_3/SiO_2$ precursors were prepared by a sol-gel method involving citrate complex.
- Nano sized and/or amorphous $LaFeO_3$ on SiO_2 particles were formed upon calcination.
- High surface area and porous texture were obtained for the formed nanocomposites.
- The work links the colloidal and surfaces phenomena to the nanocomposites formation.

GRAPHICAL ABSTRACT

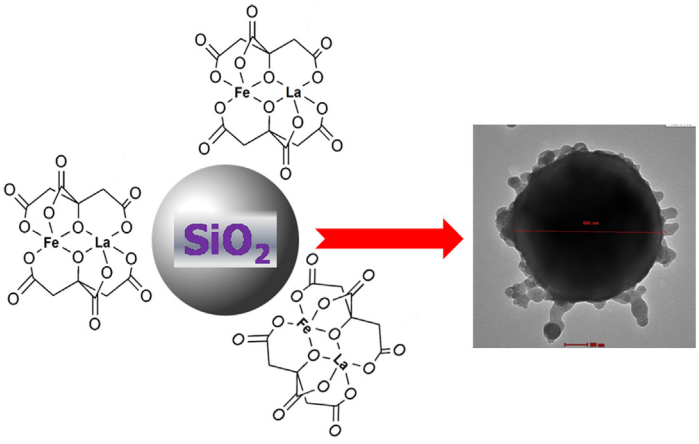

ARTICLE INFO

Article history:
Received 30 May 2016
Received in revised form 21 July 2016
Accepted 24 July 2016
Available online 26 July 2016

Keywords:
Perovskite
$LaFeO_3$
mixed oxide
nanocomposite
Porosity

ABSTRACT

A series of 10, 20 and 30% (w/w) La_2O_3-Fe_2O_3/silica composites were synthesized by mixing of La-Fe citrate complex gels with spherical silica sols. This was followed by calcination of the formed xerogel at 550 °C and 750 °C for 3 h. The materials were characterized by XRD, simultaneous thermal analyses (TGA-DTA), FTIR, N_2 gas adsorption/desorption isotherms at −196 °C, and TEM techniques. Results indicated complete decomposition of the precursor complex upon calcination and development of porous composites with high surface area. However, processing of the La-Fe citrate complex gel or the silica precursors without mixing led to formation of $LaFeO_3$ perovskite oxide type and silica with very low surface area amounting to 4 and 11 m^2/g, respectively. Thus the process led to the formation of nano-sized amorphous-like $LaFeO_3$ phase (as a shell) on the surface of the spherical silica particles (core). The enhancement of surface area and porosity of the composites was correlated to the dispersion of La-Fe precursor on the surface of silica sol. The method can be generalized for other mixed oxides.

1. Introduction

Mixed metal oxides, perovskite, of the general formula ABO_3, are very interesting materials in catalytic oxidation/reduction reactions [1], photocatalytic reactions [2], and membrane preparation

* Corresponding Author.
E-mail address: kms.khalil@yahoo.co.uk (K.M.S. Khalil).

http://dx.doi.org/10.1016/j.colsurfa.2016.07.068
0927-7757/

[3]. This is owing to the low cost of their precursor materials, as well as the simplicity of their synthesis and substitution, which allows adjusting of their structure – property relationship to suit the target applications.

However, the main problems of perovskite materials in catalysis and other applications are their low surface areas and pore textural properties [4,5]. Therefore, many preparation methods have been described for increasing of surface area and porosity by employing different strategies. This involved utilization of glucose or citric acid complex methods [6–9]; as well as carbonate, oxalate, urea, maleic acid and stearic acid methods [1,4]. Among the above methods, the citrate method was the most successful one, where the low calcination temperature (~500 °C) and higher specific surface area amounting to ~30–40 m^2/g were obtained [6–10].

Moreover, some interesting methods such as auto combustion [11,12], high-energy ball milling [13,14] have been employed to obtain high surface area perovskites. Alternatively, nano sized mixed oxides, perovskites, with high surface area and porosity have been obtained through dispersion [15–17] or encapsulation [18] of suitable precursors in ordered mesoporous materials, where the host silica walls serve as barriers in inhibiting nanoparticles agglomeration.

The present work was undertaken to examine the formation of porous texture with an improved surface area via dispersion of a mixed metal oxide precursor on the surface of nonporous spherical silica (Stöber) particles. This approach has been examined for a variety of composites and/or supported materials for different applications in catalysis, [19,20], pharmaceutical [21], medical [22] and other technological applications [23–25]. In our research group we have managed preparation of many silica composites, with improved surface area and porosity such as amorphous Fe_2O_3/silica [26], CeO_2/silica [27], and TiO_2/silica [28] nanocomposites.

The present work aims preparation of $LaFeO_3$ perovskite powders by a modified simple method based on that of *Qi* et al. [11], which involve utilization of La – Fe – O citrate gel precursor. Furthermore, to enhance surface area and dispersion of the perovskite phase, the above method was extended to the preparation of $LaFeO_3$/silica composite materials. In the following, formation and characterization of the $LaFeO_3$/silica composite materials are presented.

2. Materials and methods

2.1. Materials

2.1.1. Chemicals

The following chemicals were purchased and employed as received. This includes: lanthanum(III) nitrate hexahydrate, La $(NO_3)_3.6H_2O$; iron(III) nitrate nonahydrate, $Fe(NO_3)_3.9H_2O$, (assayed), 98% (+), solid product of (Prolabo, France); citric acid, $C_6H_8O_7$ purified (Merck, India); tetraethyl orthosilicate, Si $(OC_2H_5)_4$, (TEOS), 98%, liquid, (Sigma-Aldrich Company, Ltd., (Germany); aqueous ammonia solution 33% NH_3OH (BDH, Ltd., England); Ethyl alcohol C_2H_5OH, 99.5%, (Adwic, Egypt).

2.1.2. Preparation of Blank Silica Material

The blank silica material was prepared by the method described before [27] in lights of Stöber method [29]. In brief, a 22.8 ml (0.10 mol) of TEOS was added to 205.0 ml (3.50 mol) of absolute ethanol. Ammonia solution 155.0 ml (1.50 mol) was added within 1 min, under magnetic stirring (400 r.p.m.) to induce hydrolysis of the TEOS, resulting in the formation of Stöber silica sol. The sol was maintained under continuous stirring conditions at RT for 1 h. The resultant solution was aged for a week at RT, then filtered off and dried overnight at 120 °C. The produced material was termed

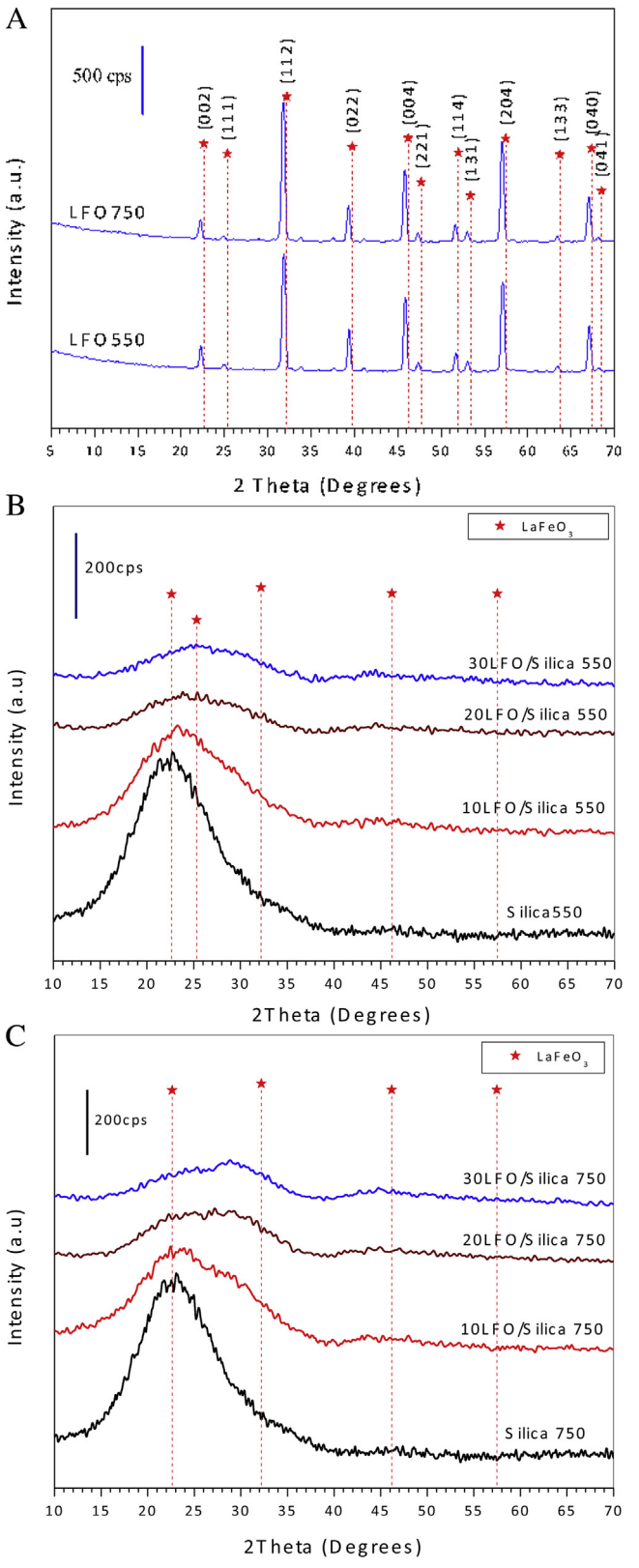

Fig. 1. XRD patterns for pure $LaFeO_3$ calcined at 550 °C and 750 °C/3 h (A); as well as for blank silica and the indicated composite materials calcined at 550 °C (B), and calcined at 750 °C (C).

as uncalcined *blank silica* 120. A portion of the uncalcined blank material was calcined at ramp rate 1 °C min^{-1} up to 550 °C, and held at this temperature for 3 h. Portion of silica calcined at 550 °C was calcined further up to 750 °C at ramp rate 10 °C min^{-1} and held at 750 °C for 3 h. The latter two materials were termed as calcined *blank silica* 550, and *blank silica* 750, respectively.

2.1.3. Preparation of Pure $LaFeO_3$

$LaFeO_3$ of perovskite type, mixed oxide structure was prepared by the sol-gel method described by Qi et al., [11] In the method, $LaFeO_3$ was prepared according to the stoichiometric composition. Thus, calculated amounts (0.010 mol) of Fe $(NO_3)_3.9H_2O$, La $(NO_3)_3.6H_2O$, and citric acid were dissolved in 25 ml distilled water. Ammonia solution (33% NH_3) was slowly added to raise pH to 7.0. The resultant sol was maintained under continuous magnetic stirring (400 r.p.m.) for 30 min at RT and then allowed to dry overnight at 90 °C. The resulted *uncalcined* citrate precursor for $LaFeO_3$ was termed as *uncalcined* LFO. Portions of the *uncalcined* citrate precursor were calcined (at ramp rate 1 °C min^{-1} up to 550 °C) similar to the above procedure to produce samples calcined at 550 °C and at 750 °C. The latter two samples were termed as *calcined* LFO550 and *calcined* LFO750, respectively.

2.1.4. Preparation of $LaFeO_3$/Silica Composites

A series of composite materials containing 10%, 20% and 30% $LaFeO_3$/Silica (w $(LaFeO_3)$/(w $(LaFeO_3)$ +w (SiO_2)) was prepared as follows. A calculated amount of Fe $(NO_3)_3.9H_2O$, La $(NO_3)_3.6H_2O$ and citric acid corresponding to 10, 20%, or 30% $LaFeO_3$/Silica was dissolved in 25 ml of distilled water. The resulted solution was transferred into a beaker containing freshly prepared Stöber silica sol, prepared by the method described above. The solution was magnetically stirred at *ca.* 400 r.p.m., and maintained under constant stirring for 1 h. The resulted solution was aged for a week at room temperature. The precipitate thus obtained was filtered off and then dried overnight at 120 °C. The resulted materials were termed *uncalcined* 10%, 20% and 30% $LaFeO_3$/Silica composites, or shortly as 10, 20, 30LFO/Silica120, respectively.

Portion of the uncalcined 10 – 30 LFO/Silica120, were calcined according to the above procedure at 550 °C and at 750 °C to produce two groups of the calcined composites. The latter two groups of samples were termed as *calcined* 10 – 30 LFO/Silica550, and 10 – 30 LFO/Silica750, respectively.

2.2. Characterization Techniques

2.2.1. X-ray Powder Diffractometry (XRD)

XRD patterns were obtained using a Phillips type Spectrometer model PW 2103/00 equipped with a Ni- filtered, employing Cu$K\alpha$ radiation (λ=1.5418 Å). The generator was operated at 35 kV and 20 mA. The diffraction patterns, derived as intensity vs. *d* spacing (Å), were compared with the relevant standards, Joint Committee on Powder Diffraction Standards (JCPDS) for identification and indexing purposes [30].

2.2.2. ATR – FTIR spectroscopy

Fourier transforms infrared (FTIR) spectroscopy for the test samples were recorded in the range of 400–4000 cm^{-1} using an instrument (Bruker-Alpha FT-IR spectrometer, Germany) equipped with a versatile high throughput horizontal ZnSe crystal for attenuated total reflactance (ATR).

2.2.3. Simultaneous Thermal Analyses

Simultaneous Thermo Gravimetric – Differential Thermal analysis (TG – DTA) of the samples carried out using a Shimadzu

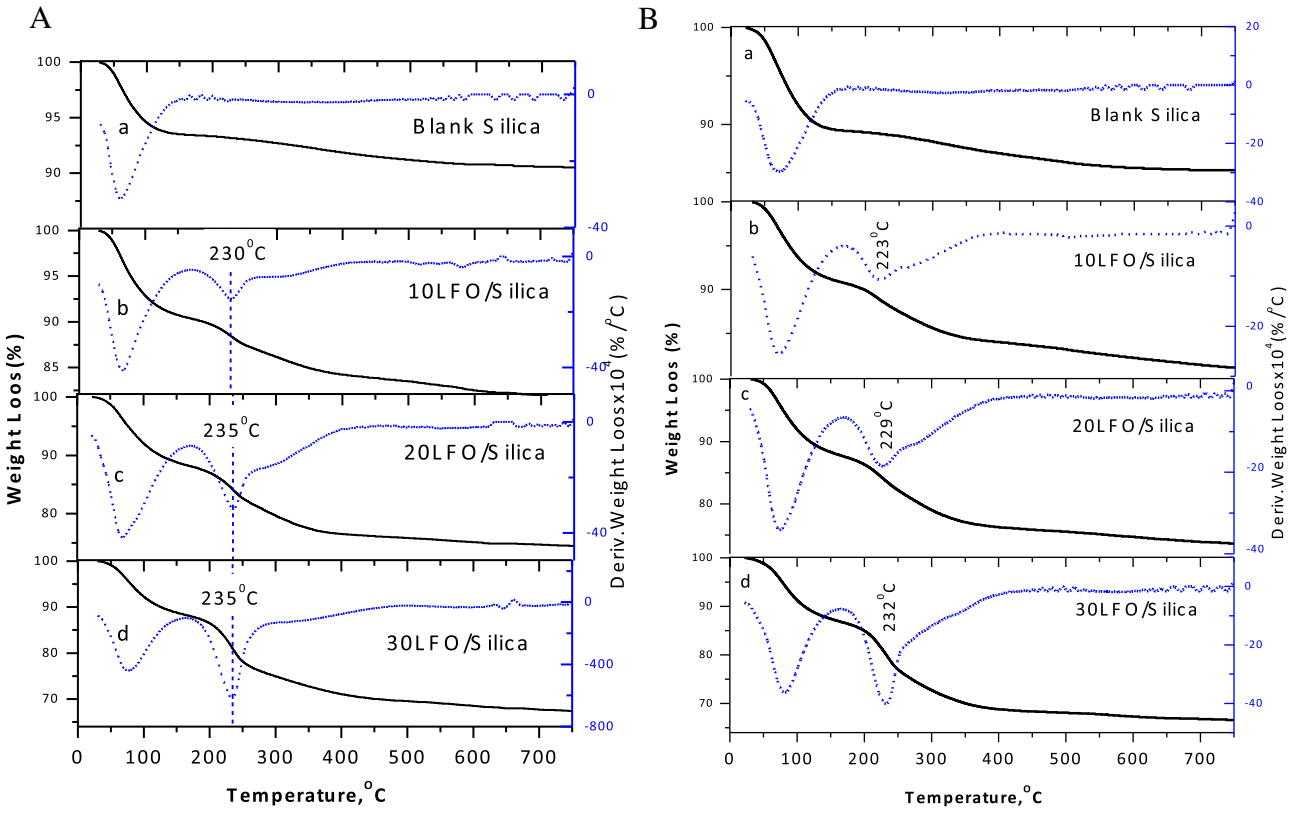

Fig. 2. TGA and DTG curves for the indicated uncalcined materials in flow of N_2 (A) and in the flow of air (B).

Simultaneous Thermal Analyzer; model DGA–60 H (Japan). Curves of TGA and DTA were recorded upon heating up to 750 °C at a heating rate of 10 °C min^{-1}, under flow of nitrogen or air atmosphere (as indicated) at the flow rate of 40 ml/min.

2.2.4. Nitrogen Adsorption and Porosity

Nitrogen adsorption/desorption isotherms at −196 °C were measured using a model ASAP 2010 instrument (Micromeritics Instrument Corporation, U.S.A.). Prior to measurement, test samples were degassed for 2 h at 200 °C to 0.1 Pa. The specific surface area, S_{BET}, was calculated by applying the famous Brunauer −Emmett-Teller (BET) equation. Pore width distribution was generated by the Barrett-Joyner-Halenda (BJH) [31]; all the measurement and related analyses were performed in the light of the IUPAC regulations [32].

2.2.5. Transmission Electron Microscopy (TEM)

For TEM measurements, samples were prepared by ultrasonic dispersion of the solid in ethanol. A drop of the resulting suspension was dropped onto a carbon-coated copper mesh grid and allowed to dry before imaging, which was carried out using a Joel 2000 instrument operated at 100 kV.

3. Results and Discussion

3.1. XRD Diffraction Patterns

XRD patterns for the pure LFO calcined at 550 °C and 750 °C materials are shown in Fig. 1A. The patterns show clearly the formation of $LaFeO_3$ phase for the material calcined at 550 °C or 750 °C. XRD of the 10 – 30 LFO/Silica composites along with pure silica; calcined at 550 °C or 750 °C are shown in Fig. 1(B and C), respectively. The patterns are, clearly, dictated by the amorphous nature of silica. Nevertheless, there is some line broadening at the position of the main diffraction lines for $LaFeO_3$ (card No., 74-2203). No additional peaks or line broadening were observed at positions characteristic for the single oxides (La_2O_3 and Fe_2O_3), or $La_2Si_2O_7$. Nevertheless, intensity of the broad peak at $2\theta = 25°$, characteristics of amorphous silica, was gradually decreased with the increasing of the LFO loading percentage. This is probably due to extensive coverage of silica particles with $LaFeO_3$ phase, which absorb radiation. It should be noted that, the disappearance of $LaFeO_3$ peaks in XRD has been normally occurred when perovskite or some other oxide phase dispersed on an ordered mesoporous [4,33] or non porous silica materials [34]. This was attributed to the absence of $LaFeO_3$ crystallites or due to the dispersion of the material as a nano sized phase below the detection limits of XRD, or due the weak $LaFeO_3$ reflections are overlapped by the strong reflections of the silicalite crystals. In light of these results it is reasonable to suggest the formation of nano sized or amorphous $LaFeO_3$ phase within the silica particles. The presence of $LaFeO_3$ in silica matrixes will be confirmed as follows.

3.2. Simultaneous TG – DTA Analyses

TGA and DTG curves for the uncalcined composite materials 10, 20 and 30LFO/Silica along with the blank SiO_2 in the flow of N_2 or air atmosphere are shown in Fig. 2(A and B), respectively. Total weight losses for the uncalcined composite along with the blank SiO_2, over the temperature range of RT–750 °C were 9.4, 18.3, 25.5 and 32.6% in the flow of N_2 (14.7, 18.9, 26.4 and 33.4% in the flow of air), respectively. This indicates that the weight loss ratio increased

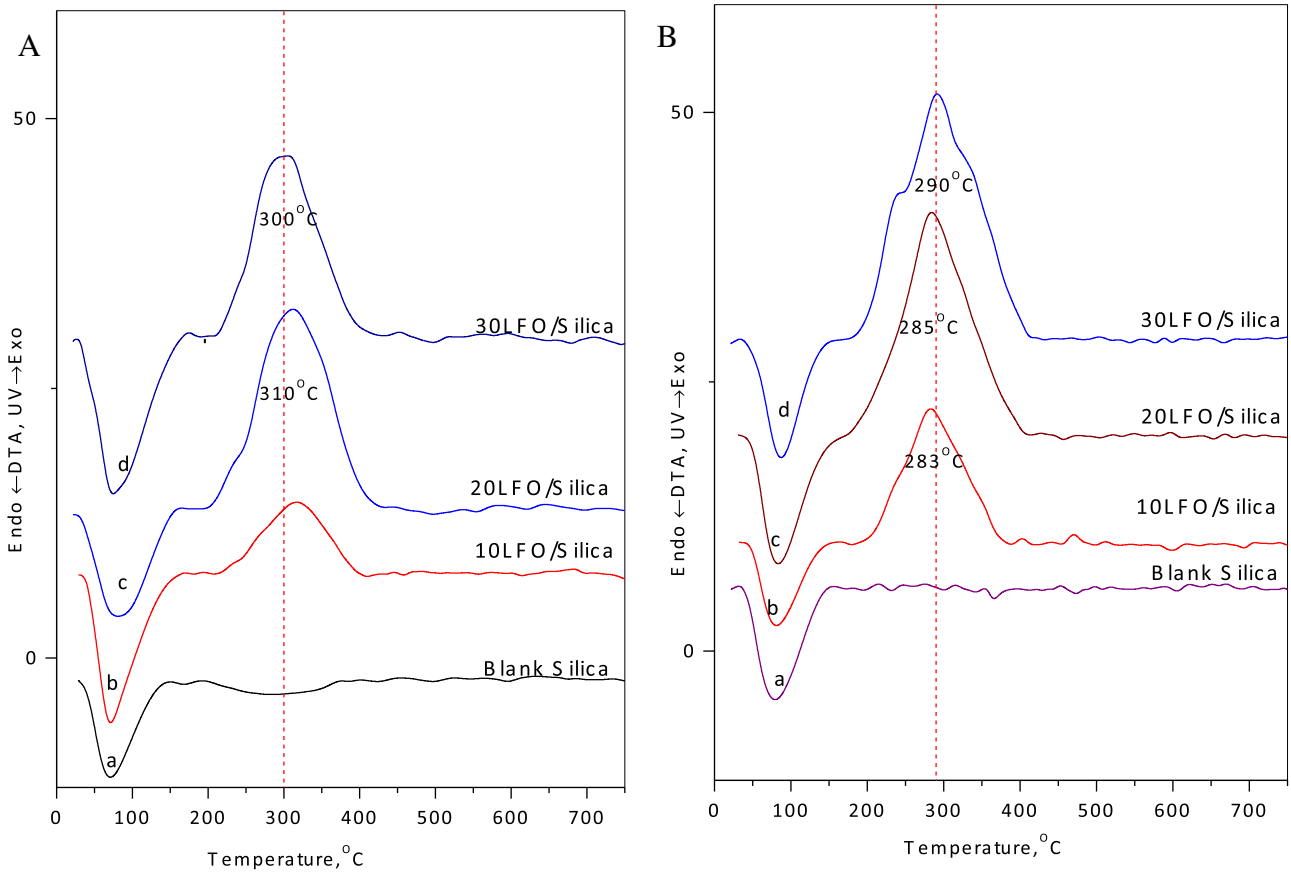

Fig. 3. DTA curves for the indicated uncalcined materials in the flow of N_2 (A) and in the flow of air (B).

with increasing of the loading ratio of the La-Fe-O citrate precursor. Moreover, TGA curves for pure silica shows a stable mass in the range of (200–750 °C) but mass loss was continued through most of this range for the composite materials. Therefore, the observed weight losses above 200 °C are surely related to the La-Fe-O citrate precursor.

DTG curves for 10, 20 and 30LFO/Silica demonstrate three steps in each curve, which can be explained as follows. The first step below 170 °C is assignable to loss of adsorbed water. The second step in the range of 170 – 400 °C, maximizes at 229 –235 °C with a shoulder at 305 °C (in the flow of N_2) and weigh loss amount to ~6.1–17.3%. In the flow of air, the second step showed little higher weight loss ~ 6.7 –17.9%, which maximize nearly at the same position 223 – 232 °C but the shoulder shifted to 280 °C. In both cases, the intensity of the shoulder peak decreases with increasing of La-Fe-O citrate precursor ratio. This helps assigning of this main DTG peak and the shoulder for the decomposition of ammonia/nitrate species and the combustion of residual organic matter, respectively. Theses assignments are in agreement with those indicated [11] for the decomposition of a similar L – F – O citrate complex.

The third step in the range of 400 – 750 °C, with weigh loss amount to 2.5 – 3.6%, appeared without any peak. In flow of air weight loss amounting to 2.9 – 2.2%, was observed in this range also without any peak, and can be assigned for structural dehydroxylation of silica. No major decomposition step related to the precursor was observed in this region.

The simultaneous DTA curves obtained with the above TGA curves in the flow of N_2 and air are shown in Fig. 3(A and B), respectively. The curves showed one main endothermic peak at < 100 °C related to the desorption of adsorbed water. Moreover, a large exothermic DTA peak maximizes ~310 °C, which was proceeded by a small exothermic shoulder (at ~ 235 °C) was observed. Thus, the main DTA peak and its preceding shoulder may be assigned for the combustion of the organic matter and the decomposition of ammonia/nitrate species, respectively. This can be confirmed by DTA results in the flow of air, where a similar exothermic peak assigned for combustion process was observed (at 285 °C). The DTA peaks were getting larger and shifted towards lower temperature (due to the presence of air instead of N_2 gas). Thus, the preceding shoulder, which assigned for the decomposition of ammonia/nitrate species was developed at ~ 235 °C (with no shift to lower temperature) which confirms the decomposition nature of such thermal event. It should be noted that no other peaks were observed at higher temperatures that related to the crystallization of bulk $LaFeO_3$ or decomposition of any other phase. More results are cited in Table 1, which indicate, the formation of stable mixed oxide phase by the end of the second thermal region (~ 500 °C) in each case.

3.3. FTIR Spectra

ATR FTIR spectra of uncalcined pure silica along with 10%, 20%, 30% LFO/Silica composites are shown in Fig. 4(A). The spectra exhibit a group of bands similar to the bands assigned to silica gel [27]. Typically, the band observed at 3203 cm^{-1} corresponds to the ν (O – H) mode of H – bonded water molecules; the band at 948 cm^{-1} corresponds to n(Si – OH); the bands at 1070 and 801 cm^{-1} correspond to ν_{as} (Si – O – Si) and ν_s (Si – O – Si) modes, respectively; and the band at 457 cm^{-1} corresponds to the δ (Si – O – Si) mode. Most important is that with the increasing of LFO precursor loading ration, two bands at 1574 cm^{-1} and 1420 cm^{-1} were developed, which were not observed for the pure silica. These peaks may be assigned to adsorbed $-COO^-$ species, and the bi – dentate nature can be expected from the large difference between the values of each peak.

FTIR spectra for the blank and composites 10 – 30% LFO/Silica550 are shown in Fig. 4(B). The spectra indicate that

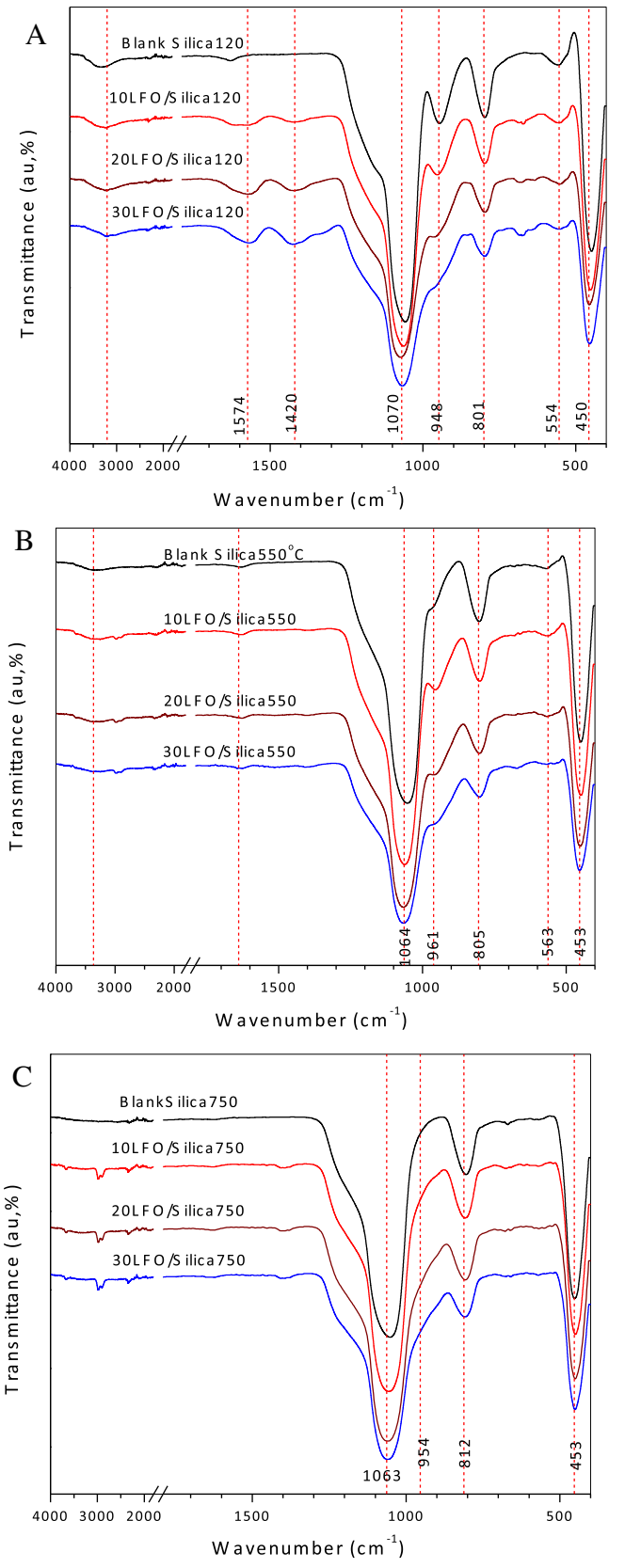

Fig. 4. ATR-FTIR spectra of the indicated uncalcined materials (A), calcined at 550 °C (B) and calcined at 750 °C (C).

Table 1
TGA—DTA Results for the uncalcined blank silica and LFO/Silica materials obtained in the flow of N_2 and in dried air flow.

Samples	N_2 flow				Air flow			
	Range (°C)	Δ W (%)	DTG Peak, °C	DTA Peak, °C	Range (°C)	Δ W (%)	DTG Peak, °C	DTA Peak, °C
Blank SiO_2	RT-150	6.5	62	71	RT-170	10.7	73	
	150-750	3.0			170-750	4.0		
	RT-750	9.5			RT-750	14.7		
10LFO/Silica120	RT-170	9.7			RT-170	9.3		
	170-400	6.1	230		170-400	6.7	223	
				317			265	283
	400-750	2.5			400-750	2.9		
	RT-750	18.3			RT-750	18.9		
20LFO/Silica120	RT-169	11.8			RT-169	12.4		
	170-400	11.7	235	310	170-400	11.3	229	
			305				280	285
	400-750	2.0			400-750	2.7		
	RT-750	25.5			RT-750	26.4		
30LFO/Silica120	RT-163	11.7			RT-169	13.3		
	163-400	17.3	235		169-400	17.9	232	245
				300			285	290
	400-750	3.6			400-750	2.2		
	RT-750	32.6			RT-750	33.4		

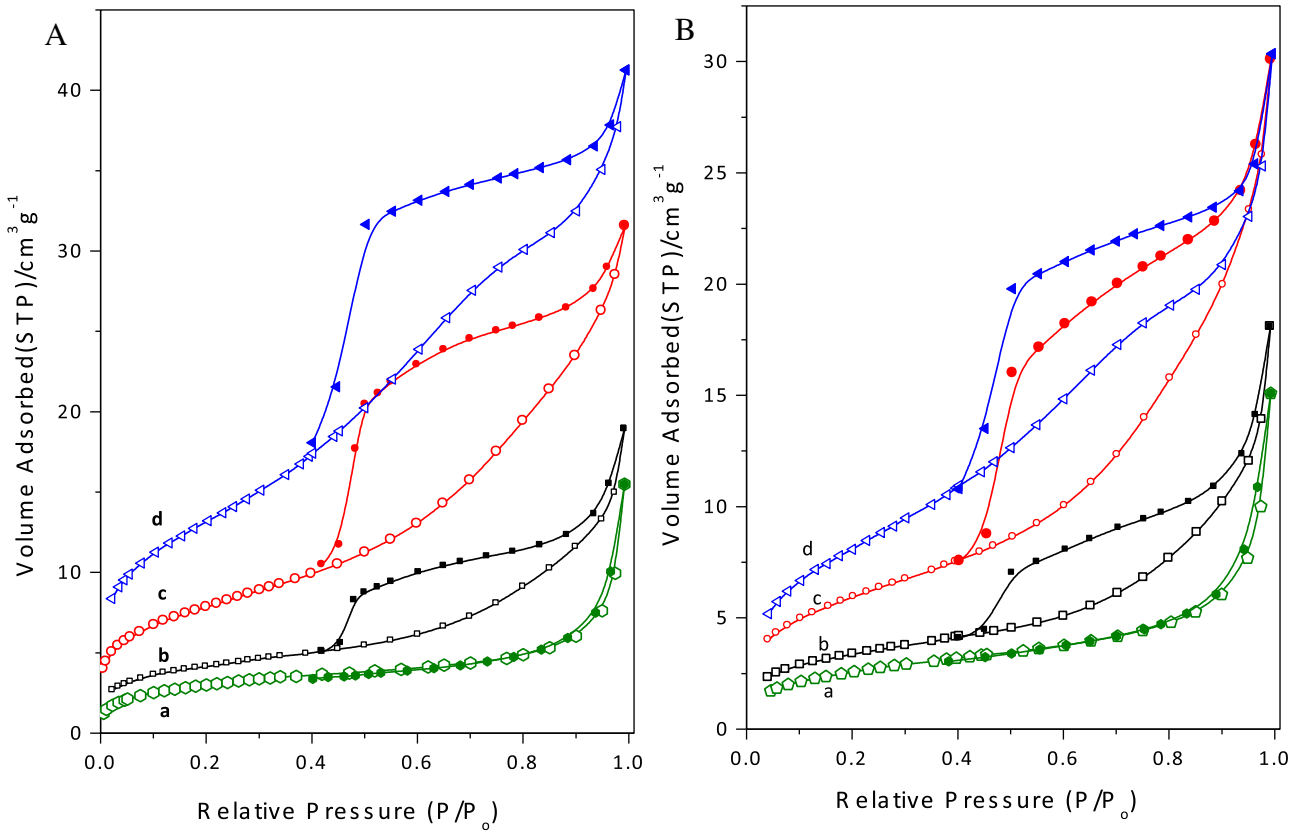

Fig. 5. N_2 adsorption/desorption isotherms for blank silica and the indicated composite materials calcined at 550 °C (A), and calcined at 750 °C (B) as indicated: a (Blank Silica), b (10LFO/Silica), c (20LFO/Silica), and d (30LFO/Silica).

the bands related to adsorbed water, nitrate, citrate or carbonate species were completely removed. Whereas, the bands characteristic for silica gel were preserved for the groups of composite materials calcined at 550 °C. Thus, pure mixed oxide phase was only present in terms of the FTIR method. Similar results were observed in the composite materials calcined at 750 °C, Fig. 4(C).

3.4. Nitrogen Adsorption, Surface Area and Porosity

Nitrogen adsorption/desorption isotherms for 10 – 30 LFO/Silica composites calcined at 550° C and 750° C along with the corresponding calcined blank silica materials, are shown in Fig. 5(A and B), respectively. According to the original IUPAC classification, the isotherm obtained with the blank silica is pure type II

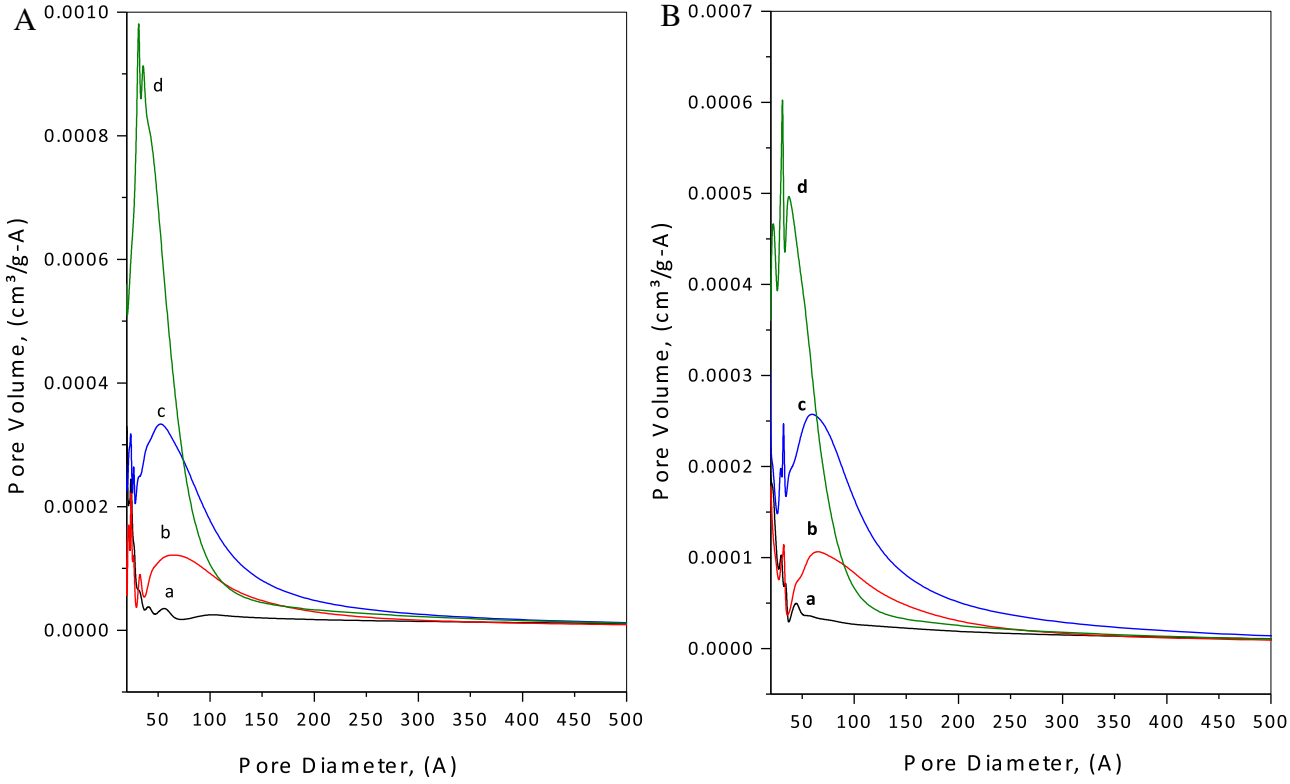

Fig. 6. Pore size distribution for blank silica and the indicated composite materials calcined at 550 °C (A), and calcined at 750 °C (B) as indicated a (blank Silica), b (10LFO/Silica), c (20LFO/Silica), and d (30LFO/Silica).

of isotherm without any obvious hysteresis loop. However, the isotherms obtained with LFO/Silica550 materials are of mixed nature and show a hysteresis loop (characteristics for type IV) at low p/p_o; while showing unlimited adsorption nature near the saturation pressure of nitrogen (characteristics of type II). Therefore, the isotherms are classified as Type $IV_{b,}$ of isotherm according to the extended classification of adsorption isotherms [35]. It can be recognized that with increasing of the LFO loading ratio, the hysteresis loops are getting wider, the surface area, S_{BET}, values and total pore volume, V_p, are getting higher, reaching 47.6 m^2g^{-1}, and 0.0638 cm^3, respectively for the 30LFO/Silica. Similar behaviors were observed for the 750 °C calcined materials. However, slightly lower S_{BET} and V_p values were obtained for the latter group due to sintering caused by calcination at such high temperature, 750 °C. Thus, a surface area reaching 30.2 m^2g^{-1}, and total pore volume, V_p amounting to 0.0469 cm^3, were obtained for the 30LFO/Silica750 composite materials.

The above results, indicate that the S_{BET} values increased by increasing the of the loading percentage, and decreased by increasing of calcination temperature from 550° C to 750° C. This suggests that gradual loading of LFO precursor led to its aggregation on the surface of nonporous silica particles, which led to the creation of porosity between adjacent silica particles.

Further texture details including results of *t*–method as external, S_t, and micro, S_{mic}, pore surface area analysis, total pore volume, V_p, and pore width, W_p, obtained via the average $4\,V_p/S_{BET}$ method as well as BJH method, were obtained and cited in Table 2. For the different materials, the *t*–plot analysis indicates that instead of the small surface area and micrporosity for blank silica and the 10LFO/Silica; larger surface area and mesoporous materials for 20 and 30 LFO/550 as well as LFO/750 were obtained. Noting that the total pore volume for the calcined blank silica550 and 750, are amount to 0.0118 and 0.0233 cm^3g^{-1}, respectively. It is evident that the increasing of porosity was due to the composite formation.

Pore size, W_P via the average $(4\,V_P/S_{BET})$ as well as BJH methods were obtained and values of peak maximum were cited in Table 2. Pore width distribution, *PWD*, obtained with blank silica and 10 – 30LFO/Silica550 and 10 – 30LFO/Silica750 are shown in Fig. 6(A and B), respectively. It is clear that the area below each PWD increases with increasing of loading ratios either for the 550 or 750 °C calcined composite groups. This indicates the creation of more porosity with increasing of the LFO loading ratio. The distribution maximizes at 108, 104, 77 and 56 Å, for the blank, 10, 20 and 30 LFO/Silica 550, respectively. PWD for the group of composites calcined at 750° C maximizes at 125 Å, 115, 91 and 64 Å for the blank, 10, 20 and 30 LFO/Silica750, respectively. Moreover, the results obtained with the average method were in agreement with the values obtained with the BJH method.

3.5. Transmission Electron Microscopy (TEM)

A typical transmission electron micrograph for the 30LFO/Silica750 composite material, is shown in Fig. 7A. From the image it is easy to recognize the presence of LFO phase domains (as aggregates of smaller irregular particles) at or/on the surface of regular spherical silica particles. The latter regular spherical morphology particle size was in the range of 200–600 nm. Careful TEM investigations showed that with lower LFO loading ratios, the amount of such irregular domains were decreased. Further investigation of the case of LFO of a silica particle was performed for a typical particle at higher magnification, Fig. 7(B). It is easy to recognize that the LFO phase domains are truly irregular and amorphous in nature. Thus, the micrograph confirms the presence of the loaded mixed oxide aggregates as irregular amorphous particles on the outer surface of the spherical silica particles.

The above work showed that the present procedure has managed composite formation through dispersion the La-Fe-O citrate gel complex on the silica surface, which was followed by drying

Table 2
Textural characteristics of the pure and composite materials calcined at 550 °C and 750 °C.

Material	$S_{BET}/(m^2g^{-1})$	C_{BET}	$V_{p/(cm^3g^{-1})}$	t-method (m^2g^{-1})		Pore width $W_p/(Å)$	
				S_{mic}	S_t	$4V/S_{BET}$	BJH
$LaFeO_3$ 550	4.0	–	–	–	–	–	–
Blank silica550	11.1	67	0.0118	0.2	10.9	42	108
10LFO/Silica550	15.2	113	0.0205	3.9	11.3	54	104
20LFO/Silica550	28.6	99	0.0406	4.1	24.5	56	77
30LFO/Silica550	47.6	102	0.0638	0.5	47.1	53	56
Blank Silica750	9.4	65	0.0233	0.1	9.3	98	125
10LFO/Silica750	12.2	94	0.0279	2.9	9.3	91	115
20LFO/Silica750	21.8	72	0.0465	2.3	19.5	85	91
30LFO/Silica750	30.2	56	0.0469	0	32.2	62	64

S_{BET} = specific surface area by BET method.
C_{BET} = *C constant of the BET equation.*
V_p = *total pore volume measured at* $p/p_o = 0.95$.

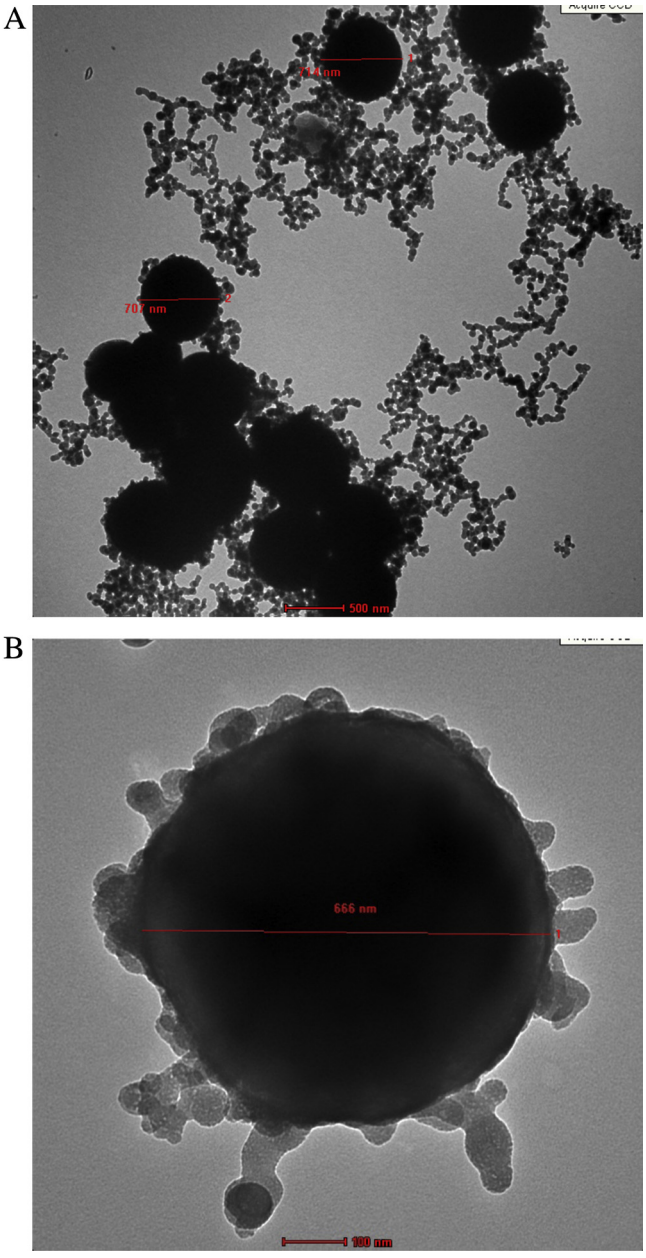

Fig. 7. TEM micrograph for general morphology of the 30LFO/Silica calcined at 750 °C (A); and a higher magnification TEM micrograph for a typical $LaFeO_3$/Silica particle.

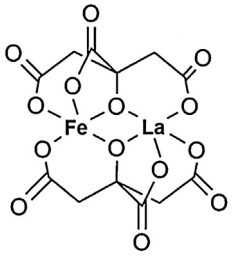

Scheme 1. Schematic representation of the complex occurs between La and Fe metallic ions with citric acid ligands (L).

and calcination at a slow ramp rate of 1 °C/min. The composite formation can be easily justified by the simple fact that while both of $LaFeO_3$ and silica were nonporous with very low surface area, reasonably high surface area and porosity were developed upon composite formation.

In fact the chemistry of citric acid complex is rather complex, not only for mixed metal but even for single metal ion. Citrate chemistry was found to be complicated and giving of a definitive description of its aqueous species at neutral pH remains elusive. Nevertheless, Silva et al., [36] has shown that ferric citrate gives a large number of species in aqueous solution. However a simplified mixed metal citric acid complex of the formula $[LaFe\ (Cit)_2]^{-2}$, can be postulated, Scheme 1, in terms of what has been suggested [36] for iron citrate as $[Fe_2\ (Cit)_2]^{-2}$, i.e. M_2L_2 complex. This complex led directly to well crystalline $LaFeO_3$ formation (but with very low surface area). When this complex was dispersed in silica sols, it supposes to form hyroxo and/or oxo complexes at pH ≥ 7.0 and allows mixed hydroxide/oxide citrate complex formation. Subsequently, the latter is due to interact with the fully hydroxylated silica surfaces. This might allow some sort of strong interaction with silica surfaces, which upon calcination stabilize the LFO phase and protect it from aggregation.

However, in spite of the rather wealth of data reported for the preparation and bulk characterization of perovskite materials, little has been reported on its texture. The present work represents full textural characterization of the composite materials. Moreover, a comparison with some available reported data [7–9,37] is shown in Table 3. Thus, it is easy to realize that the present procedure permits formation of reasonably high surface area composites. The open core and shell morphology of the composite materials make them readily for many applications in catalysis and purification purposes. Moreover, the gel nature of the precursor allows its applications as ceramic coat, powders or pellets, which increases the value of the present procedure.

Table 3
Comparison between surface areas of the different reported citrate method for pure $LaFeO_3$ or similar perovskite.

Perovskite	Calcination temperature	m^2/g	Reference
$LaFeO_3$	600 °C	38.7	[9]
$La_{0.095}Ce_{0.05}CoO_3$	700 °C/2h	32.4	[7]
$La_{0.8}Ca_{0.2}FeO_3$	N/A	38.0	[6]
$LaFeO_3$	600 °C/2h	5.2	[37]

4. Conclusions

From the above results and discussion, it is easy to conclude the following points.

1 The La-Fe-O citrate complex led directly to the formation of well crystalline $LaFeO_3$ formation, but with a very low surface area (~4.0 m^2/g).
2 Dispersion of the La-Fe-O citrate complex in silica sols, allows mixed hydroxide/oxide, citrate complex formation, which interacts strongly with the fully hydroxylated silica surfaces. This allows some sort of strong interaction with silica surfaces, which upon calcination stabilize the LFO phase and protect it from aggregation.
3 Supporting of a perovskite phase on the surface of nonporous silica led to the creation of mesoporous texture with enhanced surface area and porosity.
4 Formation of amorphous phase and the retardation of perovskite phase crystallization may be occurring due to the presence of organic citrate complex.
5 The present approach may be generalized to other perovskite systems which will lead to the formation of highly dispersed composite materials.

References

[1] S. Royer, D. Duprez, F. Can, X. Courtois, C. Batiot-Dupeyrat, S. Laassiri, et al., Perovskites as substitutes of noble metals for heterogeneous catalysis: Dream or reality, Chemical Reviews. 114 (2014) 10292–10368.
[2] E. Grabowska, Selected perovskite oxides: Characterization preparation and photocatalytic properties-A review, Applied Catalysis B: Environmental. 186 (2016) 97–126.
[3] D.D. Athayde, D.F. Souza, A.M.A. Silva, D. Vasconcelos, E.H.M. Nunes, J.C. Diniz da Costa, et al., Review of perovskite ceramic synthesis and membrane preparation methods, Ceramics International. 42 (2016) 6555–6571.
[4] S.V. Nguyen, V. Szabo, D. Trong On, S. Kaliaguine, Mesoporous silica supported LaCoO3 perovskites as catalysts for methane oxidation, Microporous and Mesoporous Materials. 54 (2002) 51–61.
[5] K. Ji, H. Dai, J. Deng, L. Song, S. Xie, W. Han, Glucose-assisted hydrothermal preparation and catalytic performance of porous LaFeO3 for toluene combustion, Journal of Solid State Chemistry. 199 (2013) 164–170.
[6] G. Pecchi, M.G. Jiliberto, E.J. Delgado, L.E. Cadús, J.L.G. Fierro, Effect of B-site cation on the catalytic activity of La1-xCaxBO3 (B = Fe, Ni) perovskite-type oxides for toluene combustion, Journal of Chemical Technology & Biotechnology. 86 (2011) 1067–1073.
[7] Y. Wu, L. Luo, Preparation of La0.95Ce0.05CoO3 with large surface area, Indian Journal of Chemistry. 48 (2009) 202–205.
[8] M. Soleymani, A. Moheb, E. Joudaki, High surface area nano-sized La0.6Ca0.4MnO3 perovskite powder prepared by low temperature pyrolysis of a modified citrate gel, Central European Journal of Chemistry. 7 (2009) 809–817.
[9] S. Nakayama, $LaFeO_3$ perovskite-type oxide prepared by oxide-mixing, co-precipitation and complex synthesis methods, Journal of materials Science 6 (2001) 5643–5648.
[10] L.G. Fierro, J.L.G. Tejuca (Eds.), In Properties a Nd Applications of Perovskite-type Oxides, 6, Marcel Dekker Inc., New York, 1993.
[11] X. Qi, J. Zhou, Z. Yue, Z. Gui, L. Li, Short communication A simple way to prepare nanosized LaFeO 3 powders at room temperature, Ceramics International. 29 (2003) 347–349.
[12] G. Tesquet, J. Faye, F. Hosoglu, A.-S. Mamede, F. Dumeignil, M. Capron, Ethanol reactivity over La1+x FeO3+δ perovskites, Applied Catalysis A: General. 511 (2016) 141–148.
[13] M.Y. Leiw, G.H. Guai, X. Wang, M.S. Tse, C.M. Ng, O.K. Tan, Dark ambient degradation of Bisphenol A and Acid Orange 8 as organic pollutants by perovskite $SrFeO_3$ metal oxide, Journal of Hazardous Materials. 260 (2013) 1–8.
[14] L.G. Pinaeva, L.A. Isupova, I.P. Prosvirin, E.M. Sadovskaya, I.G. Danilova, D.V. Ivanov, et al., La–Fe–O/CeO_2 Based Composites as the Catalysts for High Temperature N2O Decomposition and CH4 Combustion, Catalysis Letters. 143 (2013) 1294–1303.
[15] N. Wang, X. Yu, Y. Wang, W. Chu, M. Liu, A comparison study on methane dry reforming with carbon dioxide over LaNiO3 perovskite catalysts supported on mesoporous SBA-15, MCM-41 and silica carrier, Catalysis Today. 212 (2013) 98–107.
[16] M.-J. Suh, Y.-K. Park, S.-K. Ihm, One-pot synthesis of perovskite-type metal oxides via confined mesopore and their catalytic activity for toluene oxidation, Catalysis Today. 265 (2016) 210–217.
[17] H. Li, J. Zhu, P. Xiao, Y. Zhan, K. Lv, L. Wu, et al., On the mechanism of oxidative degradation of rhodamine B over LaFeO3 catalysts supported on silica materials: Role of support, Microporous and Mesoporous Materials. 221 (2016) 159–166.
[18] K. Niu, L. Liang, J. Li, F. Zhang, Efficient encapsulation of $LaCoO_3$ perovskite in mesoporous silica induced by a chelating template, Microporous and Mesoporous Materials. 220 (2016) 220–224.
[19] K.X. Yao, H.C. Zeng, Simultaneous Chemical Modification and Structural Transformation of Stöber Silica Spheres for Integration of Nanocatalysts, Chemistry of Materials. 24 (2012) 140–148.
[20] K.S. Shin, Y.K. Cho, J.-Y. Choi, K. Kim, Facile synthesis of silver-deposited silanized magnetite nanoparticles and their application for catalytic reduction of nitrophenols, Applied Catalysis A: General. 413-414 (2012) 170–175.
[21] T. Gholami, M. Salavati-Niasari, M. Bazarganipour, E. Noori, Synthesis and characterization of spherical silica nanoparticles by modified Stöber process assisted by organic ligand, Superlattices and Microstructures. 61 (2013) 33–41.
[22] C. Li, C. Ma, F. Wang, Z. Xi, Z. Wang, Y. Deng, et al. Preparation and Biomedical Applications of Core?Shell Silica/Magnetic Nanoparticle Composites, Journal of Nanoscience and Nanotechnology 12 (2012) 2964–2972.
[23] J. Zhu, S. Wei, N. Haldolaarachchige, D.P. Young, Z. Guo, Electromagnetic Field Shielding Polyurethane Nanocomposites Reinforced with Core–Shell Fe–Silica Nanoparticles, The Journal of Physical Chemistry C 115 (2011) 15304–15310.
[24] R. Epherre, E. Duguet, S. Mornet, E. Pollert, S. Louguet, S. Lecommandoux, et al., Manganite perovskite nanoparticles for self-controlled magnetic fluid hyperthermia: about the suitability of an aqueous combustion synthesis route, Journal of Materials Chemistry. 21 (2011) 4393.
[25] P. Lu, J.-L. Zhang, Y.-L. Liu, D.-H. Sun, G.-X. Liu, G.-Y. Hong, et al., Synthesis and characteristic of the Fe_3O_4@SiO_2@Eu(DBM)$_{3.2}H_2O$/Silica luminomagnetic microspheres with core-shell structure, Talanta. 82 (2010) 450–457.
[26] K.M.S. Khalil, H.A. Mahmoud, T.T. Ali, Direct formation of thermally stabilized amorphous mesoporous Fe2O3/Silica nanocomposites by hydrolysis of aqueous iron III nitrate in sols of spherical silica particles, Langmuir: The ACS Journal of Surfaces and Colloids. 24 (2008) 1037–1043.
[27] K.M.S. Khalil, L.A. Elkabee, B. Murphy, Formation and characterization of different ceria/Silica composite materials via dispersion of ceria gel or soluble ceria precursors in silica sols, Journal of Colloid and Interface Science. 287 (2005) 534–541.
[28] K.M.S. Khalil, A.A. Elsamahy, M.S. Elanany, Formation and characterization of high surface area thermally stabilized titania/silica composite materials via hydrolysis of titanium(IV) tetra-isopropoxide in sols of spherical silica particles, Journal of Colloid and Interface Science. 249 (2002) 359–365.
[29] W. Stöber, A. Fink, E. Bohn, Controlled growth of monodisperse silica spheres in the micron size range, Journal of Colloid and Interface Science 26 (1968) 62–69.
[30] JCPDS, International Centre for Diffraction Data, PCPDFWIN, JCPDS-ICDD. (1995).
[31] E.P. Barrett, L.G. Joyner, P.H. Halenda, The Determination of Pore Volume and Area Distributions in Porous Substances, I. Computations from Nitrogen Isotherms, J. Am. Chem. Soc. 73 (1951) 373–380.
[32] K.S.W. Sing, D.H. Everett, R.A.W. Haul, L. Moscou, R.A. Pierotti, J. Rouquérol, et al., International Union of Pure Commission on Colloids and Surface Chemistry and Catalysis Reporting physisorption data for Gas/Solid Systems with Special Reference to the Determination of Surface Area and Porosity, Pure & Appl Chem. 54 (1982) 2201–2218.
[33] A. Ramanathan, R. Maheswari, D.H. Barich, B. Subramaniam, Niobium incorporated mesoporous silicate, Nb-KIT-6: Synthesis and characterization, Microporous and Mesoporous Materials. 190 (2014) 240–247.
[34] S. a. Karakoulia, K.S. Triantafyllidis, a. a. Lemonidou, Preparation and characterization of vanadia catalysts supported on non-porous, microporous and mesoporous silicates for oxidative dehydrogenation of propane (ODP), Microporous and Mesoporous Materials. 110 (2008) 157–166.
[35] F. Rouquerol, J. Rouquerol, K. Sing, 'Adsorption by Powders & Porous Solids', Academic Press, London, 1999.
[36] A.M.N. Silva, X. Kong, M.C. Parkin, R. Cammack, R.C. Hider, Iron(III) citrate speciation in aqueous solution, Dalton transactions (Cambridge, England 2009 (2003) 8616–8625.
[37] K. Rusevova, R. Köferstein, M. Rosell, H.H. Richnow, F.-D. Kopinke, A. Georgi, LaFeO3 and BiFeO3, perovskites as nanocatalysts for contaminant degradation in heterogeneous Fenton-like reactions, Chemical Engineering Journal 239 (2014) 322–331.